The Innovation

Report

Coupled deep-mantle carbon-water cycle: Evidence from lower-mantle diamonds

Wenzhong Wang,[1,6,7,*] Oliver Tschauner,[2] Shichun Huang,[2] Zhongqing Wu,[1,3] Yufei Meng,[4] Hans Bechtel,[5] and Ho-Kwang Mao[4]
*Correspondence: wz30304@mail.ustc.edu.cn
Received: December 1, 2020; Accepted: April 30, 2021; Published Online: May 4, 2021; https://doi.org/10.1016/j.xinn.2021.100117

Graphical abstract

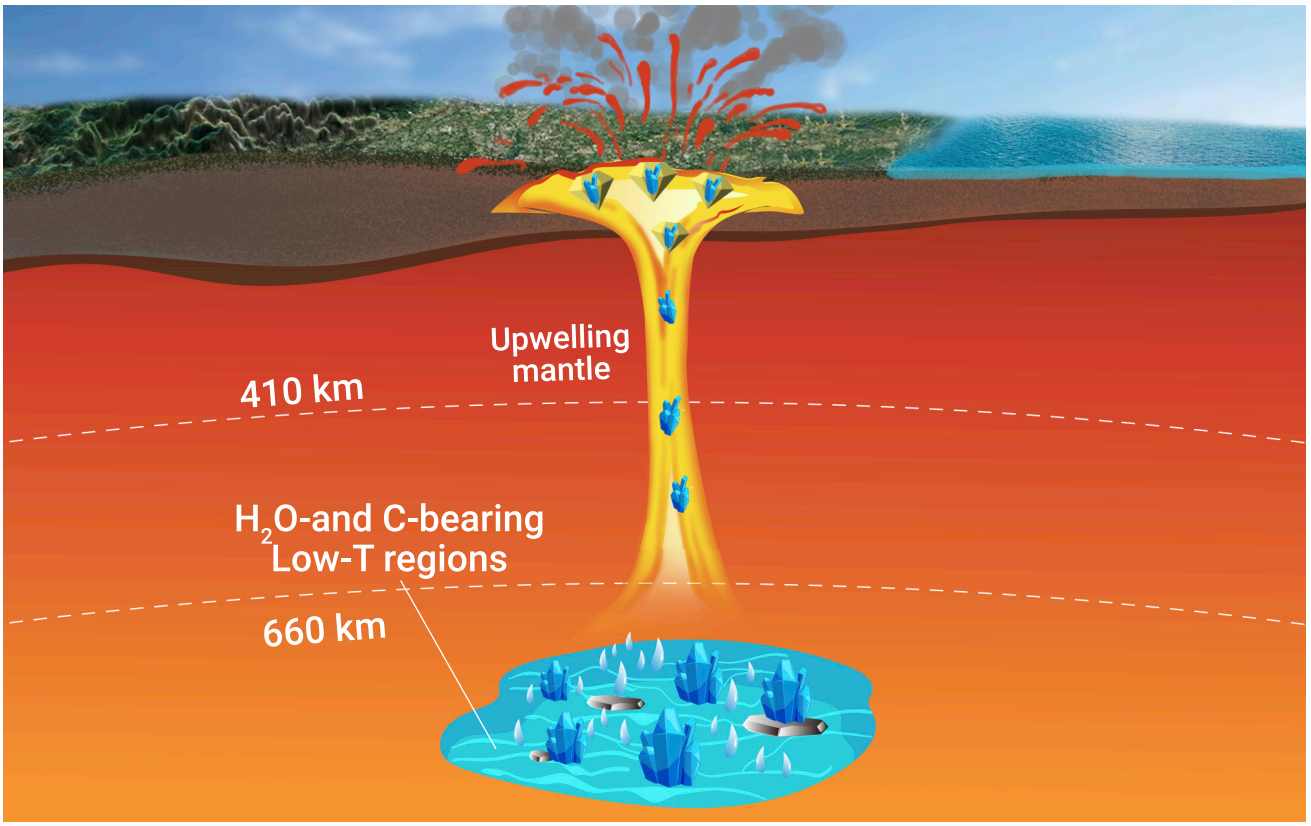

Public summary

- A novel approach was developed to assess the pressure-temperature conditions of entrapment of inclusions in diamonds
- The viscoelastic relaxation of diamond has a significant effect on the evolution of pressure and temperature
- Ice-VII-bearing diamonds have formed in wet, cool environments at depths down to 800 km
- The coupled recycling of water and carbon is present in the deep mantle

Report

Coupled deep-mantle carbon-water cycle: Evidence from lower-mantle diamonds

Wenzhong Wang,[1,6,7,*] Oliver Tschauner,[2] Shichun Huang,[2] Zhongqing Wu,[1,3] Yufei Meng,[4] Hans Bechtel,[5] and Ho-Kwang Mao[4]

[1]Laboratory of Seismology and Physics of Earth's Interior, School of Earth and Space Sciences, University of Science and Technology of China, Hefei 230026, China
[2]Department of Geoscience, University of Nevada Las Vegas, Las Vegas, NV 89154, USA
[3]CAS Center for Excellence in Comparative Planetology, USTC, Hefei, Hefei 230026, China
[4]Center for High Pressure Science and Technology Advanced Research, Shanghai 201203, China
[5]Advanced Light Source, Lawrence Berkeley National Laboratory, Berkeley, CA 94720, USA
[6]Department of Earth Sciences, University College London, London WC1E 6BT, UK
[7]Earth and Planets Laboratory, Carnegie Institution for Science, Washington, DC 20015, USA
*Correspondence: wz30304@mail.ustc.edu.cn

Received: December 1, 2020; Accepted: April 30, 2021; Published Online: May 4, 2021; https://doi.org/10.1016/j.xinn.2021.100117

Citation: Wang W., Tschauner O., Huang S., et al., (2021). Coupled deep-mantle carbon-water cycle: Evidence from lower-mantle diamonds. The Innovation **2(2)**, 100117.

Diamonds form in a variety of environments between subducted crust, lithospheric and deep mantle. Recently, deep source diamonds with inclusions of the high-pressure H_2O-phase ice-VII were discovered. By correlating the pressures of ice-VII inclusions with those of other high-pressure inclusions, we assess quantitatively the pressures and temperatures of their entrapment. We show that the ice-VII-bearing diamonds formed at depths down to 800 ± 60 km but at temperatures 200–500 K below average mantle temperature that match the pressure-temperature conditions of decomposing dense hydrous mantle silicates. Our work presents strong evidence for coupled recycling of water and carbon in the deep mantle based on natural samples.

Keywords: diamond; deep mantle; water and carbon cycle; first-principles calculations

INTRODUCTION

Decades of effort in geodynamic modeling and seismic observations have confirmed the presence of lateral heterogeneities in the transition zone (TZ) and lower mantle (LM) of Earth.[1–3] These heterogeneities are distinguished through reduced seismic velocities and seismic wave reflections and can be generated by the presence of melt or fluid,[3] or by thermal and chemical variations in the mantle.[4,5] In this context, diamonds provide key information because some of them contain inclusions that were entrapped in the TZ or LM,[6–11] and, hence, are part of the global deep-carbon cycle. Generally, diamond formation is not bound to subduction. The vast majority of diamonds, including most of the diamonds that we have examined, have formed in the subcontinental lithosphere without direct relation to subduction processes. However, the release of carbonaceous material from subducted slabs can result in the formation of diamond in a reducing mantle through a reaction of enstatite with magnesite[12] or at greater depth through comproportionation of carbon from carbonate and carbide.[13,14] Iron carbide has been proposed to be an abundant accessory mineral in the mantle at depths where the pressure-induced disproportionation of Fe^{2+} into Fe^0 plus Fe^{3+} dominates the redox conditions.[13] This mechanism finds support in the frequent occurrence of iron and iron carbide inclusions in diamonds from deep mantle.[10,15,16]

Recently, the discovery of hydrous ringwoodite[8] and ice-VII[10] as inclusions in diamonds has correlated the question of water storage in the deep mantle with the carbon cycle. It was also shown that some inclusions in diamonds sustain remnant pressures of several gigapascals (GPa),[9,10] high enough to imply formation in the TZ or LM. Hence, these inclusions provide direct mineralogical information about the TZ and LM, whereas products of retrograde transformations of high-pressure minerals[6,7] conserve composition but no fully quantifiable information about the pressure-temperature (P-T) conditions of their entrapment. Here, we show that diamonds with inclusions of ice-VII and other minerals at high remnant pressure not only represent entrapment in environments rich in carbonaceous aqueous fluid, which permit the formation of diamond[13] and ice-VII,[10] but that they generally represent very cool environments within the LM, above the solidus of wet carbonated peridotite but below the solidus of wet peridotite, and are in apparent correlation with the decomposition boundary of dense hydrous Mg silicate phase D.

Our approach is based on the *in situ* observation of μm- to sub-μm scale mineral inclusions in diamonds which bear remnant pressures in the range of 2–14 GPa (Table 1; Figure 1). These remnant pressures define foot points of their P-T paths that these inclusions experienced between the time of their entrapment in growing diamond and presence.[9,10,17] Inclusions that were entrapped at the same depth in the Earth have P-T paths intersecting at the same P-T point. Here, we use a new concept of correlating P-T paths of different inclusions in one diamond for assessing the P-T of entrapment (see the materials and methods). This approach is different from earlier assessments which involve a priori assumption about the geotherm.[9,18,19] At the same time, we take full account of the viscoelastic relaxation of the host diamond (see the supplemental methods). In our approach, assessment of the P-T paths is in two steps: first through the condition of the equal strain of host diamond and inclusions (isomeke,[17] which we call here "elastic paths" to emphasize the abstraction from viscoelastic relaxation) and, second, the role of viscoelastic relaxation of diamond.[20,21] Finally, we show that accounting for viscoelastic relaxation gives temperatures that match the average mantle residence temperatures obtained from nitrogen defects in diamond,[22] which give estimates of average residence temperatures as a function of residence time.[22] In our approach, P and T are strictly correlated. Thus, independent confirmation of T also confirms that the assessment of P is correct.

RESULTS

The information about diamonds investigated in this work is described in detail in the supplemental methods. We conducted X-ray diffraction measurements on the inclusions. The diffraction and X-ray fluorescence data of ilmenite (ilm>95) and taenite (Fe50Ni50) from Diamantina-1 gave the following volumes: 307.9(5) and 44.9(3) $Å^3$, respectively. The Fe/Mg ratio of ilmenite was assessed through Rietveld refinement and the Fe/Ni ratio of taenite through the integrated intensity ratio of the Fe and Ni Kα lines using the LARCH program.[27] The diffraction data of the ice-VII bearing Orapa samples had been reported in Tschauner et al.[10] Published composition, volumes, and diffraction data of a garnet-ilmenite-TAP (10 Å phase)-liebermannite inclusion in diamond ON-ZIZ-74[25] are included in Table 1 because they provide a cross-check of the present method with conventional garnet geobarometry.[26,28,29] In addition, we measured the infrared spectra of the diamonds

Table 1. Pressures and temperatures from the adiabatic approach compared with temperatures from nitrogen aggregation[22] (second column from the right) using ages from Chaves et al.[23,24] and Timmerman et al.[23,24]

	Nitrogen aggregation				Adiabatic P-T	
Specimen	A (ppm)	B (ppm)	Age (Ga)	T (K)	T (K)	P (GPa)
Orapa GRr1507	94 ± 9	49 ± 7	0.9–1.6	1,430 ± 30	1,420 ± 20	28.6 ± 1.4
Orapa GRr1519	87 ± 9	53 ± 7	0.9–1.6	1,430 ± 20	1,490 ± 50	23.3 ± 2.0
Orapa M57666	96 ± 6	68 ± 7	0.9–1.6	1,460 ± 20	1,442 ± 40	29.0 ± 2.0
Diamantina	52 ± 12	134 ± 15	>1.7	1,460 ± 30	–	11.6 ± 0.6[a]
ON-ZIZ74	55 ± 8	13 ± 1	-[b]	1,450 ± 50	–	14.5 ± 0.5[b]

Further details are given in the supplemental methods.
[a]Pressure from elastic P-T paths and temperature from N aggregation.
[b]Unknown age but a residence time of 0.1 Ga corresponds to 1,490 ± 10 K while 3 Ga give 1,400 ± 10 K.[25] P and T were assessed through the intersection of isomeke of ilmenite with the geobarometer pressure of coexisting garnet.[25,26].

and used the calibrations by Boyd et al.[30,31] for estimating the amount of nitrogen in A- and B-type defects, respectively. The amount of D-type defects was found to be less than 10 ppm in any specimen based on the calibration by Clark and Davey[32] and was neglected as being within uncertainties of the amounts of A-type and B-type defects. The nitrogen contents from A- and B-type defects range from 52 to 96 ppm and from 49 to 134 ppm, respectively. The corresponding percentage of A-type defects and the approximate age of the diamonds (Table 1) were used to estimate average mantle residence temperatures.[23,24] The fitted defect profiles and observed spectra are shown in Figure S1. Nitrogen contents and estimated mantle residence temperatures are presented in Table 1.

Remnant 300 K pressures of inclusions were assessed from their unit cell volumes corrected for the elastic relaxation of diamond at 300 K.[17] The corrected pressures were used as foot points for calculations of P-T paths for the inclusions based on the condition of the equilibrated strain of inclusion and diamond (elastic path). In a second step, the paths were corrected for viscoelastic relaxation of the hosting diamond.

DISCUSSION

We start with discussing the common case of annealed inclusion-diamond systems. Temperatures near the average mantle adiabat[33] are well above the temperatures of viscoelastic relaxation of diamond.[20,21] This observation was already made by Anzolini et al.[19] for assessing the entrapment pressure of a periclase inclusion in a diamond. Thus, P-T of inclusions and their hosting diamond equilibrate with the surrounding mantle and follow a nearly adiabatic path upon ascent until the temperature drops below the brittle-to-viscous transition in diamonds. This is illustrated in Figure 1A for inclusions in a type IaB diamond from the Diamantina alluvial deposits. The remnant pressures of the inclusions are 1 and 4 GPa, respectively, at 300 K, which are remnant pressure values typically found for the super-deep diamonds from Juina, Brazil, that formed at least within the TZ or deeper.[19] The elastic P-T paths of ilmenite and taenite intersect right at the viscoelastic limit of diamond of 1,200–1,300 K[20,21] above 9.8 GPa (Figure 1A). Any memory of the P-T path above that limit is lost, although we can use the percentage of remnant A-type defects in this diamond to estimate temperature[22] and the elastic P-T path to estimate a minimum P of entrapment (Figure 1A; Table 1), which is consistent with the Ni content of the taenite inclusions of this diamond.[34] Another example is the inclusion of garnet, ilmenite, TAP, and liebermannite in diamond ON-ZiZ74a (Table 1), which has been reported previously.[25] The elastic path of ilmenite intersects the geobarometric pressure of garnet based on its majorite component,[28,29] leading to an estimated P-T condition of 14.5 ± 0.5 GPa and 1,450 ± 50 K, which is only slightly above the boundary of the elastic-to-viscoelastic transition of diamond.[25] The assessed entrapment P-T condition is consistent with the Ca and ferric Fe content of this garnet,[26] the phase stability of liebermannite, and the average residence temperature of the hosting diamond obtained using nitrogen content. We expect to find this convergence of the elastic P-T paths at the elastic-viscoelastic transition of diamond for deep-mantle inclusions in general. In fact, diamonds from Juina and Kankan, which originated in the deep mantle, contain inclusions that formed retrogradely from higher pressure minerals,[6,7] or high-pressure minerals relaxed to low remnant pressure,[8] in accordance with viscoelastic relaxation over extended geologic time at a depth shallower than the depth of entrapment. This long relaxation time is also reflected in the extended annealing of nitrogen defects to virtually only type B[9] or N-free type II diamonds.[6,7]

However, some diamonds contain inclusions whose elastic release P-T paths do not intersect at the elastic-to-viscoelastic transition in diamond but noticeably at higher pressure and temperature (Figure 1B). These sustained pressure differences within the viscoelastic regime clearly show that these inclusions did not experience full relaxation in viscoelastically deforming diamond upon ascent and that they conserve an at least partial record of their actual P-T conditions of entrapment in the deeper mantle. More precisely, these diamonds have ascended at rates higher than that which allows complete viscoelastic relaxation of their host diamonds. One may argue that such an intersection at high P-T could be incidental. However, the elastic P-T paths of inclusions in diamonds are quite steep (Figure 1). Hence, their intersection at a pressure within mantle P-T mathematically implies that their entrapments have occurred within a limited pressure range in the mantle: elastic P-T paths of inclusions of clearly different origins, such as lithospheric inclusions in fibrous rims or along cracks compared with inclusions in the kernel of these diamonds, do not intersect at a positive temperature or within any plausible P-T bounds.

We can use the sustained pressure differences of high-pressure inclusions to constrain the actual P-T conditions of entrapment. We examine two limiting cases: (1) intersection of the elastic P-T paths and (2) convergence along an adiabatic path based on the observed excess pressure at the diamond viscoelastic limit (Figure 1B; for further details, see the supplemental methods). As a check, we estimate T independently through the N aggregation state in the diamonds.[22] We find that the adiabatic path gives the same temperatures as the N aggregation in their host diamonds within uncertainties (Table 1; Figure 2). Therefore, the adiabatic path provides plausible temperature estimates for the inclusions. In contrast, the elastic paths markedly overestimate T and underestimate P. Along an adiabatic path P and T are correlated. Therefore, with T independently confirmed, our approach also provides reliable estimates of P.

The results are summarized in Figure 2. All P-T points are above the solidus of wet carbonated peridotite.[35] All diamonds with ice-VII inclusions fall within a P-T range between the solidi of wet and wet carbonated peridotite,[35] but quite below the solidus of dry carbonated[13] or even alkaline-rich peridotite.[36] Notably, all P-T points are tied to wet cool environments at depths down to 820 km, and temperatures of 200–500 K below a reference average mantle adiabat.[33] This finding is consistent with the formation of these diamonds in the surrounding of cold slabs (Figure 2). Below ~800 km depth the P-T points of entrapment are at the decomposition line of the dense hydrous magnesium silicate phase D,[37] suggesting that the presence of H_2O, which is now conserved as ice-VII, and the formation of the hosting diamond

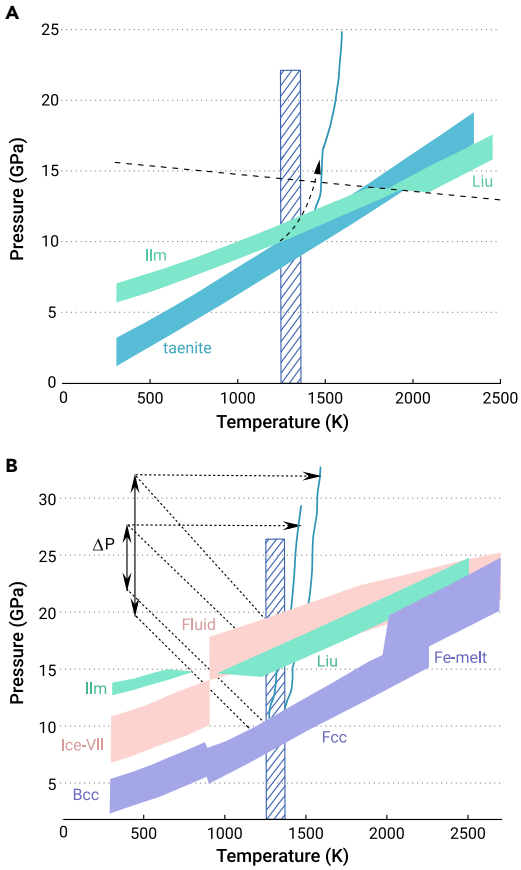

Figure 1. P-T paths of high-pressure inclusions in diamonds (A) Inclusions of ilmenite (ilm>95, geik<5) and taenite (Fe50Ni50) observed in a diamond from the Diamantina alluvial deposits (see the supplemental methods). The calculated elastic release paths start to intersect at the diamond viscoelastic limit (hachured area). This indicates that the inclusions were in elastic equilibrium with the host diamond above this limit. Above this limit, P-T is expected to have evolved close to a mantle adiabat (blue line). The ilmenite-liuite phase boundary is indicated. (B) Inclusions of ilmenite (ilm92geik7) and iron (Fe>95) in a diamond from Orapa, Botswana. The range of foot pressures and P-T paths reflect the uncertainties (see the supplemental methods). Offsets of paths are the results of phase transformations. The blue hachured region indicates the transition from elastic-to-viscoelastic deformation of diamonds. We assess the corresponding T through the intersection of a reference adiabat (blue) with P + ΔP (indicated through dashed lines). This P + ΔP and T gives a lower limit of P-T of entrapment. However, the temperature of this lower limit matches the temperature estimate from nitrogen defect distribution in this diamond (Table 1). This shows that the lower limit represents the actual P-T path quite closely.

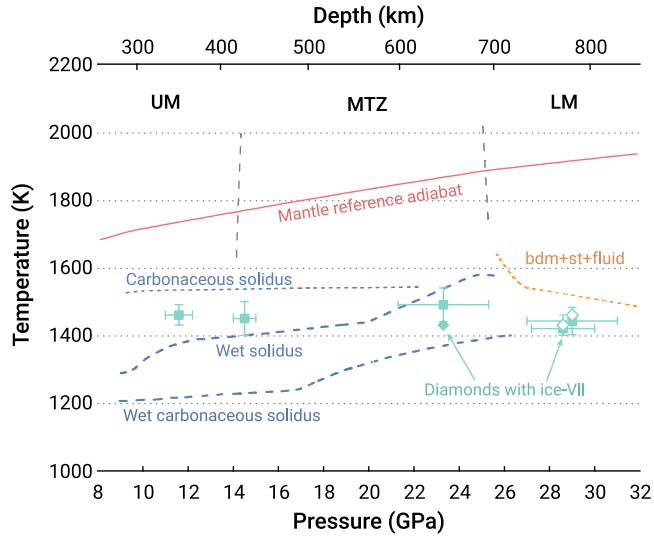

Figure 2. P-T points of entrapment of inclusions in diamonds Blue squares, assessment based on adiabatic approach; hollow diamonds, temperature assessed through nitrogen aggregation. Reference mantle adiabat is from Brown and Shankland,[33] carbonaceous, wet, and wet-carbonaceous solidus of peridotite are from Tschauner et al.,[10] Litasov et al.,[35] and Ghosh et al.[36] The decomposition boundary of phases D to bridgmanite (bdm), stishovite (st), and fluid was taken from[37]. All inclusions were entrapped in diamonds which grew in cool wet environments down to 820 km depth. Consistent with experiments, these diamonds grew above the solidus of C-H-O fluid-bearing peridotite.[35] The formation of these diamonds is tied to local wet areas in the TZ[38] and dehydration of phases B and D[37] above ~800 km.

are correlated with the decomposition of hydrated mantle silicate. Metallic iron in the same diamonds may be a remnant of the redox-reaction mechanism proposed by Rohrbach and Schmidt,[13] which, therefore, may be active within the LM. Preservation of high remnant pressure and an overall low-temperature regime and short residence time in the mantle are correlated: the sample with the longest mantle residence time (from Diamantina, Table 1) has kept no record of a P-T path beyond the elastic deformation regime of diamond. In many deep-source diamonds, long residence at temperatures above the elastic-viscoelastic limit of diamond has removed the record of their origins beyond the observation of transformation products of former high-pressure phases. However, the observation of hydrous minerals,[8,25,39] taenite, and iron as inclusions in ultradeep-source diamonds[8,10,15] point toward a common origin at 500–800 km depth but different paths and timescales of ascent (Figure 2). It cannot be excluded that diamonds form at even greater depth. Equally well, remnant water may be kept in the mantle to even greater depth,[37] but we show that water present at the depth of 800 ± 60 km is still involved in the recycling of water and carbon (as witnessed through the diamonds) (Figure 2). This concept is shown in a carton (Figure 3). This does not imply that all deep-mantle diamonds formed in similarly wet environments or that certain deep layers in Earth are globally wet. Nevertheless, we establish a conjunction between these conditions within the LM, the deep-carbon, and the deep-water cycle.

Conclusion

We have developed a novel approach to assess the entrapment P-T conditions of inclusions with high remnant pressure in diamonds. Similar to Anzolini et al.,[19] we find that the viscoelastic relaxation of diamond has a significant effect on the evolution of P and T of inclusions. The results show that ice-VII-bearing diamonds have formed in wet, cool environments at depths down to 820 km and temperatures of 200–500 K below the average mantle geotherm. This is consistent with the formation of these diamonds in the surrounding of cold slabs. This work presents evidence for the recycling of water and carbon in the deep mantle, even to the LM.

MATERIALS AND METHODS

X-ray diffraction and X-ray fluorescence analysis

X-ray diffraction data were collected at beamlines 13-IDB, -IDE, and 34-IDE at energies of 30, 19, and 22 keV, respectively. The primary beams were focused by elliptical mirrors to micrometer scale (34-IDE: 0.5 μm) beam diameters. Diffraction data were collected with area detectors, calibrated, and integrated with Dioptas. X-ray fluorescence was excited by the same primary beams and collected with a Vortex detector. The diffraction data of the Orapa samples had been reported previously (see online depository of Tschauner et al.[10]). The diffraction- and X-ray fluorescence data of ilmenite (ilm>95) and taenite (Fe50Ni50) from Diamantinas-1 gave the following volumes: 307.9(5) and 44.9(3) Å^3. The Fe-Ni ratio of taenite- and iron-inclusions was assessed using the LARCH program.[27]

Infrared spectra of the examined diamonds

The spectra of all samples except GRR 1521 were collected in transmission at beamline 1.4, ALS, with a Nicolet Magna 760 FTIR bench and a Nic-Plan IR microscope with a 32× magnification Schwarzschild objective, with 1 cm^{-1} resolution and a HgCdTe detector with a KBr beam splitter. Apertures were set to 20 × 20 to 40 × 60 μm^2 spatial resolution. The spectrum of the sample Diamantina-1 was obtained from the uncut specimen. The spectrum of GRr1521 was taken from a crushed, clear piece with a Thermo-Nicolet iS50 FTIR at the mineral spectroscopy laboratory at Caltech in transmission with a glow bar source and 2 cm^{-1} resolution. All other spectra

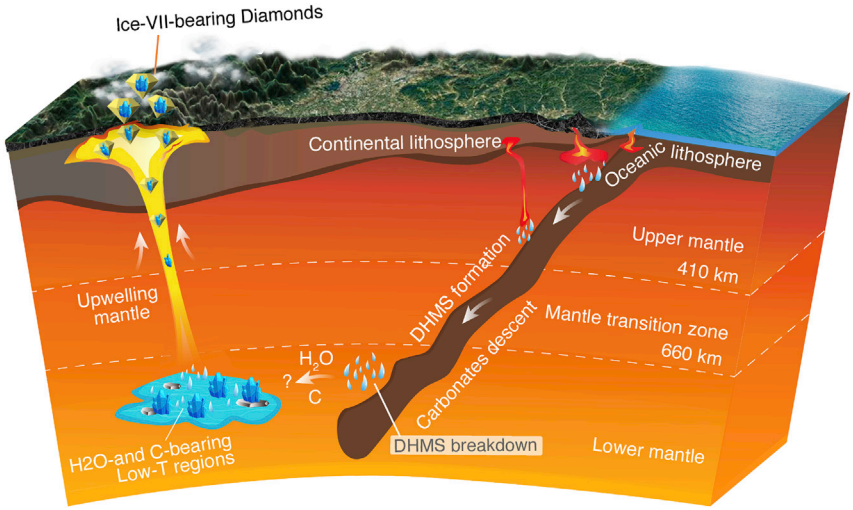

Figure 3. Schematic diagram of the formation of ice-VII-bearing diamonds in the deep mantle Ice-VII-bearing diamonds present in this study have formed at wet cool environments at depths down to 820 km and temperatures of 200–500 K below the average mantle geotherm. Below ~800 km depth the P-T points of entrapment are at the decomposition line of the dense hydrous magnesium silicate phase D,[37] indicating that the presence of H_2O, which is now conserved as ice-VII, and the formation of the hosting diamond may be related to the dehydration of hydrated mantle silicate in subducted slab. The deep mantle formed ice-VII-bearing diamonds may continue growing at lithosphere depth, as evidenced by many low to ambient pressure inclusions of chromite, pyroxenes, sellaite, or methane hydrate in their rims.

were obtained from laser-cut, polished platelets. A synthetic type II diamond was used for assessing absorbance between 1,000 and 1,500 cm^{-1}. Spectra were background subtracted and scaled to an equal thickness of 10 mm. Contributions of A-, B-, and D-type defect bands were assessed by using the pure defect-type spectra reported by Taylor et al.[22] We used the calibrations by Boyd et al.[30,31] for estimating the amount of nitrogen in A- and B-type defects, respectively. The amount of D-type defects was found to be less than 10 ppm in any specimen based on the calibration by Clark and Davey[32] and was neglected as being within uncertainties of the amounts of A- and B-type defects. The nitrogen contents from A- and B-type defects, the corresponding percentage of A-type defects, and the approximate age of the diamonds (Table 1) were used to estimate average mantle residence temperatures.[23,24] These temperatures are used as comparison with the temperatures obtained from the modeled P-T paths. The N content in the hosting diamonds may be locally lower and such variations cannot be clearly seen in transmission IR spectroscopy but we found that the temperatures obtained from P-T paths are not systematically different from the estimates based on N defects. The fitted defect profiles and observed spectra are shown in Figure S1. These spectra and fits correspond to the results in Table 1.

Ab initio calculations

Computational calculations were conducted using the Quantum Espresso package[40] (ilmenite and liuite[41]), Vienna ab initio simulation package (VASP)[42] plus finite displacement approach[43] for ice-VII, first-principles molecular dynamics simulations (FPMD) on the cubic box containing 210 H_2O molecules for fluid H_2O, and equation of state of iron phases from Dorogokupets et al.[44]

For ilmenite and liuite, the local density approximation (LDA) was used for assessing the exchange-correlation. The energy cutoff for electronic wave functions was set at 70 Ry. The oxygen pseudopotential was generated using the Troullier-Martins method[45] with a cutoff radius of 1.45 Bohr and a valence configuration of $2s^2 2p^4$. The pseudopotentials for iron (Fe) and titanium (Ti) were generated using the Vanderbilt method[46] with a valence configuration of $3s^2 3p^6 3d^{6.5} 4s^1 4p^0$ for iron and a valence configuration $3s^2 3p^6 3d^2 4s^2$ for titanium. The cutoff radii for both pseudopotentials are 1.8 Bohr. Due to the existence of large on-site Coulomb interactions among the localized electrons (e.g., 3d electrons),[47] we introduced a Hubbard U correction to the LDA (LDA + U). Hubbard U values for Fe and Ti atoms in ilmenite were non-empirically determined using the linear response method.[48] Crystal structures of ilmenite were well optimized using the damped variable cell shape molecular dynamics at variable pressures on a 6 × 6 × 6 k-point mesh, and vibrational density of state (VDoS) values were calculated using the finite displacement method.[43] However, the vibrational phonon calculations for liuite report some imaginary frequencies, which hampers the calculations of the high-temperature equation of state (EoS). Here, we obtained the 0 K isotherm of liuite[41] from LDA + U calculations and estimated the EoS at different temperatures using the thermal expansion of bridgmanite.[49] We assumed that temperature shows a similar effect on the volume changes of $FeTiO_3$ and $MgSiO_3$ perovskites.

Due to the failure of LDA in predicting the properties of the H_2O system,[50] we performed first-principles calculations for ice-VII and H_2O fluids by adopting the generalized gradient approximation[51] for the exchange-correlation function. All calculations for ice-VII were done using VASP code,[42] and the PBE-type of pseudopotentials for hydrogen and oxygen were used. The energy cutoff for plane waves was set as 700 eV. For solid ice-VII, relaxed crystal structures under different pressures were obtained by optimizing cell parameters and atomic coordinates at an 8 × 8 × 8 k-point mesh grid, and their VDoS values were derived from the finite displacement method.[43] For H_2O fluids, we conducted FPMD simulations on the cubic box containing 210 H_2O molecules to determine the EoS. FPMD simulations were propagated in the canonical ensemble (NVT) with a Nosé thermostat and the Brillouin zone was sampled at gamma point. All simulations on cubic boxes with variable volumes lasted at least 40,000 steps with a time step of 1.0 fs, and the temperature was set as 600, 900, 1,200, 1,500, 2,000, 2,300, 2,500, 2,700, and 3,000 K. Pressures at different temperatures and volumes can be derived by calculating ensemble averages of the instantaneous pressure after reaching the equilibrium state.

Determination of P-T paths

Remnant 300 K pressures of inclusions were assessed by synchrotron microdiffraction of their unit cell volumes at beamlines 13-IDDIDE and 34-IDD. Experimental parameters and data are provided in the supplemental information. We used empirical equations of state of the mineral inclusions for the given composition. Subsequently, the elastic relaxation of diamond at 300 K was corrected.[17] The corrected pressures were used as foot points for calculations of pressure-temperature (P-T) paths for the inclusions and the paths were calculated based on the condition of the equilibrated strain of inclusion and diamond (elastic path). We used the variance of pressures for separate inclusions of the same phase as upper and lower bounds for the foot points. Because of the low compressibility, low thermoelastic softening, and low thermal expansivity of diamond, the elastic paths are close to but not identical with isochores.[9,10] First-order phase transitions were addressed by calculating separate paths for low and high P-T phases, assessment of the pressure difference at the phase boundaries (coexistence range), and subsequent correction for diamond relaxation under isothermal conditions. The required thermoelastic parameters were obtained from *ab initio* calculations and literature data. Details of these calculations and the correction for minor chemical components are described above. By using empirical foot pressures we largely circumnavigate the issue of possible overestimation or underestimation of computed volumes from insufficient correction of electron exchange correlation. Consequently, deviations between computed and available empirical high P-T volume data are within the uncertainties of the latter. Generally, we used these deviations and the uncertainties of the foot point pressures in combination to estimate the upper and lower bounds of P-T paths (Figure 1). Uncertainties of intersection points are defined by the upper and lower intersection points of intersecting paths in P-T space.

All data are given in Tables 1 and S1–S3, and are plotted in Figures 1 and S2. Partial relaxation is a time-dependent, therefore, path-dependent process. Thus, changes in pressure, volume, and temperature are path dependent as well. In addition, partial relaxation is expected to differ for different inclusions, depending on their elastic moduli, phase transformations, and their actual sizes and shapes. We constrain this unknown time-dependent P-T path by two non-path-dependent limiting cases (Figure 1B). In case I, the intersection of the elastic P-T paths defines the upper limit of temperature and the lower limit of pressure of their entrapment P-T point because it defines the most rigid response of diamond to the stress exerted by the inclusions at a given P-T of the surrounding rock. This is shown in Figure 1B. For all examined specimens, these P-T intersection points are well above the viscoelastic limit of diamond and well above the present mantle geotherm (Figure 1B). In case II we look at the pressure differences between these inclusions at the elastic-viscoelastic transition temperature and use an adiabatic path for assessing the P-T of entrapment as a lower T limit (Figure 1B). It turns out that, within uncertainties, the adiabatic P-T paths give the same temperature as the correlation of nitrogen content in the host diamonds with the percentage of A-type defects (Table 1; Figure 2). As a low-temperature limit, we assume

that an adiabatic path intersects the viscoelastic limit temperature of 1,200–1,300 K at the lowest observed pressure of the inclusions (Figure 1B). In the case of complete relaxation, the inclusions would have the same pressure at this temperature. The observed ΔP at the diamond elastic-viscoelastic transition quantifies an excess pressure and a corresponding adiabatic ΔT (Figure 1B). The transition from brittle elastic to visco-elastic behavior of diamond has been examined for single and poly-crystals, the latter giving lower bounds. Without discussing the possible effect of N, and P-T on the yield strength, we set the viscoelastic limit to the reported temperatures for single and polycrystals. Then we define two reference adiabats from the upper and lower intersection of the elastic P-T paths with these two limits (Figure 1B) and bracket ΔP and ΔT. The validity of the adiabatic approach is confirmed through the agreement of the assessed temperatures with the temperatures obtained from N aggregation states (Figure 2; Table 1). A similar finding was reported by Anzolini et al.[19] for single periclase inclusions from the TZ.

REFERENCES

1. French, S.W., and Romanowicz, B. (2015). Broad plumes rooted at the base ofthe Earth's mantle beneath major hotspots. Nature ***525***, 95–99. https://doi.org/10.1038/nature14876.
2. Ballmer, M.D., Schmerr, N.C., Nakagawa, T., et al. (2015). Compositional mantle layering revealed by slab stagnation at 1000-km depth. Science Advances ***1***. https://doi.org/10.1126/sciadv.1500815.
3. Schmandt, B., Jacobsen, S.D., Becker, T.W., et al. (2014). Dehydration melting at the top of the lower mantle. Science ***344***, 1265–1268. https://doi.org/10.1126/science.1253358.
4. Wang, W., Xu, Y., Sun, D., et al. (2020). Velocity and density characteristics of subducted oceanic crust and the origin of lower-mantle heterogeneities. Nature communications ***11***. https://doi.org/10.1038/s41467-019-13720-2.
5. Wang, W., Liu, J., Zhu, F., et al. (2021). Formation of large low shear velocity provinces through the decomposition of oxidized mantle. Nature communications ***12***. https://doi.org/10.1038/s41467-021-22185-1.
6. Brenker, F.E., Stachel, T., and Harris, J.W. (2002). Exhumation of lower mantle inclusions in diamond: ATEM investigation of retrograde phase transitions, reactions and exsolution. Earth Planet. Sci. Lett. ***198***, 1–9.
7. Stachel, T., Harris, J.W., Brey, G.P., et al. (2000). Kankan diamonds (Guinea) II: lower mantle inclusion parageneses. Contrib. Mineral. Petrol. ***140***, 16–27.
8. Pearson, D.G., Brenker, F.E., Nestola, F., et al. (2014). Hydrous mantle transition zone indicated by ringwoodite included within diamond. Nature ***507***, 221–224.
9. Navon, O., Wirth, R., Schmidt, C., et al. (2017). Solid molecular nitrogen (δ-N_2) inclusions in Juina diamonds: exsolution at the base of the transition zone. Earth Planet. Sci. Lett. ***464***, 237–247.
10. Tschauner, O., Huang, S., Greenberg, E., et al. (2018). Ice-VII inclusions in diamonds: evidence for aqueous fluid in Earth's deep mantle. Science ***359***, 1136–1139.
11. Nestola, F., Korolev, N., Kopylova, M., et al. (2018). $CaSiO_3$ perovskite in diamond indicates the recycling of oceanic crust into the lower mantle. Nature ***555***, 237–241.
12. Luth, R.W. (1993). Diamonds, eclogites, and the oxidation state of the Earth's mantle. Science ***261***, 66–68.
13. Rohrbach, A., and Schmidt, M.W. (2011). Redox freezing and melting in the Earth's deep mantle resulting from carbon–iron redox coupling. Nature ***472***, 209–212.
14. Liu, J., Wang, W., Yang, H., et al. (2019). Carbon isotopic signatures of super-deep diamonds mediated by iron redox chemistry. Geochemical Perspect. Lett. ***10***, 51–55.
15. Smith, E.M., Shirey, S.B., Nestola, F., et al. (2016). Large gem diamonds from metallic liquid in Earth's deep mantle. Science ***354***, 1403–1405.
16. Kaminsky, F.V., and Wirth, R. (2011). Iron carbide inclusions in lower-mantle diamond from Juina, Brazil. Can. Mineral. ***49***, 555–572.
17. Angel, R.J., Mazzucchelli, M.L., Alvaro, M., et al. (2014). Geobarometry from host-inclusion systems: the role of elastic relaxation. Am. Mineral. ***99***, 2146–2149.
18. Anzolini, C., Angel, R.J., Merlini, M., et al. (2016). Depth of formation of $CaSiO_3$-walstromite included in super-deep diamonds. Lithos ***265***, 138–147.
19. Anzolini, C., Nestola, F., Mazzucchelli, M.L., et al. (2019). Depth of diamond formation obtained from single periclase inclusions. Geology ***47***, 219–222.
20. Weidner, D.J., Wang, Y., and Vaughan, M.T. (1994). Strength of diamond. Science ***266***, 419–422.
21. Yu, X., Raterron, P., Zhang, J., et al. (2012). Constitutive law and flow mechanism in diamond deformation. Sci. Rep. ***2***, 876.
22. Taylor, W.R., Jaques, A.L., and Ridd, M. (1990). Nitrogen-defect aggregation characteristics of some Australasian diamonds; time-temperature constraints on the source regions of pipe and alluvial diamonds. Am. Mineral. ***75***, 1290–1310.
23. Chaves, M.L.S.C., Karfunkel, J., Hoppe, A., et al. (2001). Diamonds from the Espinhaço range (Minas Gerais, Brazil) and their redistribution through the geologic record. J. South Am. Earth Sci. ***14***, 277–289.
24. Timmerman, S., Krebs, M.Y., Pearson, D.G., et al. (2019). Diamond-forming media through time—trace element and noble gas systematics of diamonds formed over 3 billion years of Earth's history. Geochim. Cosmochim. Acta ***257***, 266–283.
25. Huang, S., Tschauner, O., Yang, S., et al. (2020). HIMU geochemical signature originating from the transition zone. Earth Planet. Sci. Lett. ***542***, 116323.
26. Tao, R., and Fei, Y. (2021). Recycled calcium carbonate is an efficient oxidation agent under deep upper mantle conditions. Commun. Earth Environ. ***2***, 45.
27. Newville, M. (2013). Larch: an analysis package for XAFS and related spectroscopies. J. Phys. Conf. Ser. ***430***, 012007.
28. Collerson, K.D., Williams, Q., Kamber, B.S., et al. (2010). Majoritic garnet: a new approach to pressure estimation of shock events in meteorites and the encapsulation of sub-lithospheric inclusions in diamond. Geochim. Cosmochim. Acta ***74***, 5939–5957.
29. Wijbrans, C.H., Niehaus, O., Rohrbach, A., et al. (2014). Thermodynamic and magnetic properties of knorringite garnet ($Mg_3Cr_2Si_3O_{12}$) based on low-temperature calorimetry and magnetic susceptibility measurements. Phys. Chem. Miner. ***41***, 341–346.
30. Boyd, S.R., Kiflawi, I., and Woods, G.S. (1995). Infrared absorption by the B nitrogen aggregate in diamond. Philos. Mag. B ***72***, 351–361.
31. Boyd, S.R., Kiflawi, I., and Woods, G.S. (1994). The relationship between infrared absorption and the A defect concentration in diamond. Philos. Mag. B ***69***, 1149–1153.
32. Clark, C.D., and Davey, S.T. (1984). One-phonon infrared absorption in diamond. J. Phys. C Solid State Phys. ***17***, 1127–1140.
33. Brown, J.M., and Shankland, T.J. (1981). Thermodynamic parameters in the Earth as determined from seismic profiles. Geophys. J. Int. ***66***, 579–596.
34. Rohrbach, A., Ghosh, S., Schmidt, M.W., et al. (2014). The stability of Fe–Ni carbides in the Earth's mantle: evidence for a low Fe–Ni–C melt fraction in the deep mantle. Earth Planet. Sci. Lett. ***388***, 211–221.
35. Litasov, K.D., Shatskiy, A., and Ohtani, E. (2014). Melting and subsolidus phase relations in peridotite and eclogite systems with reduced COH fluid at 3–16 GPa. Earth Planet. Sci. Lett. ***391***, 87–99.
36. Ghosh, S., Ohtani, E., Litasov, K.D., et al. (2009). Solidus of carbonated peridotite from 10 to 20 GPa and origin of magnesiocarbonatite melt in the Earth's deep mantle. Chem. Geol. ***262***, 17–28.
37. Nishi, M., Irifune, T., Tsuchiya, J., et al. (2014). Stability of hydrous silicate at high pressures and water transport to the deep lower mantle. Nat. Geosci. ***7***, 224–227.
38. Wang, W., Zhang, H., Brodholt, J.P., et al. (2020). Elasticity of hydrous ringwoodite at mantle conditions: implication for water distribution in the lowermost mantle transition zone. Earth Planet. Sci. Lett. ***554***, 116626.
39. Palot, M., Jacobsen, S.D., Townsend, J.P., et al. (2016). Evidence for H_2O-bearing fluids in the lower mantle from diamond inclusion. Lithos ***265***, 237–243.
40. Giannozzi, P., Baroni, S., Bonini, N., et al. (2009). Quantum ESPRESSO: a modular and open-source software project for quantum simulations of materials. J. Phys. Condens. Matter ***21***, 395502.
41. Tschauner, O. (2019). High-pressure minerals. Am. Mineral. ***104***, 1701–1731.
42. Kresse, G., and Furthmüller, J. (1996). Efficient iterative schemes for ab initio total-energy calculations using a plane-wave basis set. Phys. Rev. B ***54***, 11169–11186.
43. Togo, A., and Tanaka, I. (2015). First principles phonon calculations in materials science. Scr. Mater. ***108***, 1–5.
44. Dorogokupets, P.I., Dymshits, A.M., Litasov, K.D., et al. (2017). Thermodynamics and equations of state of iron to 350 GPa and 6000 K. Sci. Rep. ***7***, 41863.
45. Troullier, N., and Martins, J.L. (1991). Efficient pseudopotentials for plane-wave calculations. II. Operators for fast iterative diagonalization. Phys. Rev. B ***43***, 8861–8869.
46. Vanderbilt, D. (1990). Soft self-consistent pseudopotentials in a generalized eigenvalue formalism. Phys. Rev. B ***41***, 7892–7895.
47. Anisimov, V.I., Zaanen, J., and Andersen, O.K. (1991). Band theory and Mott insulators: Hubbard U instead of Stoner I. Phys. Rev. B ***44***, 943–954.
48. Cococcioni, M., and de Gironcoli, S. (2005). Linear response approach to the calculation of the effective interaction parameters in the LDA+U method. Phys. Rev. B ***71***, 035105.
49. Shukla, G., Wu, Z., Hsu, H., et al. (2015). Thermoelasticity of Fe^{2+}-bearing bridgmanite. Geophys. Res. Lett. ***42***, 1741–1749.
50. Hamann, D.R. (1997). H_2O hydrogen bonding in density-functional theory. Phys. Rev. B ***55***, R10157–R10160.
51. Perdew, J.P., Burke, K., and Ernzerhof, M. (1996). Generalized gradient approximation made simple. Phys. Rev. Lett. ***77***, 3865–3868.

ACKNOWLEDGMENTS

This work was supported through NSF EAR-1838330, EAR-1942042, Natural Science Foundation of China (41925017, 41721002), and the Fundamental Research Funds for the Central Universities (WK2080000144). The Advanced Light Source is supported through contract no. DE-AC02-05CH11231. W. Wang acknowledges support from the UCL-Carnegie Postdoctoral Scholarship. We thank two anonymous referees for their thorough and constructive reviews, and Dr. Gaojun Li for his editorial handling.

Report

AUTHOR CONTRIBUTIONS

O.T., S.H., and W.W. conceived and designed this project. W.W. performed the theoretical calculations. W.W. and O.T. wrote the manuscript and all authors contributed to the discussion of the results and revision of the manuscript.

DECLARATION OF INTERESTS

The authors declare no competing interests.

SUPPLEMENTAL INFORMATION

Supplemental information can be found online at https://doi.org/10.1016/j.xinn.2021.100117.

LEAD CONTACT WEBSITE

https://www.researchgate.net/profile/Wenzhong-Wang-4.